ACS OMEGA

http://pubs.acs.org/journal/acsodf

Article

Ultimate Eradication of the Ciprofloxacin Antibiotic from the Ecosystem by Nanohybrid GO/O-CNTs

Mohammad M. Fares,* Fahmi A. Abu Al-Rub,* and Ahmad R. Mohammad

Cite This: *ACS Omega* 2020, 5, 4457−4468

Read Online

ACCESS | Metrics & More | Article Recommendations

ABSTRACT: Eradication of pharmaceutical drugs from the global ecosystem has received remarkable attention due to the extensive horrible consequences on the human immunological system and the high rate of human deaths. The urgent need for drug eradication became the dominant priority for many research institutions worldwide due to the sharp increase of antimicrobial resistance (AMR) in the human body, which inhibits drug effectiveness and leads ultimately to death. Nanohybrid GO/O-CNTs was fabricated from graphene oxide (GO) cross-linked via calcium ions (Ca^{2+}) with oxidized carbon nanotubes (O-CNTs) to eradicate the well-known ciprofloxacin antibiotic drug from aqueous solutions. The ciprofloxacin drug is medically prescribed in millions of medical prescriptions every year and typically exists in domestic and wastewaters. Characterization of the nanohybrid GO/O-CNTs was carried out through spectroscopic (Fourier Transform Infrared (FTIR) and X-ray diffraction (XRD)), thermal (Thermogravimetric analysis (TGA) and derivative thermogravimetry (DTG)), and microscopic (scanning electron microscopy (SEM)) techniques. Optimum parameters for the drug eradication process from aqueous solutions were verified and selected as follows: contact time = 4 h, pH = 6.0, temperature = 290 K, %$CaCl_2$ = 0.5%, GO/O-CNT ratio = 4:1, and adsorbent mass = 1.0 mg. The equilibrium data were fitted to different adsorption isotherms, and the Langmuir isotherm provided the best fit to our data. Dynamic studies demonstrated a pseudo-second-order removal process for the ciprofloxacin drug, and thermodynamic parameters confirmed exothermic drug adsorption (−27.07 kJ/mol) as well as a physisorption process. For the sake of fighting against the generated AMR, our working strategy demonstrated a removal efficiency of 99.2% of the ciprofloxacin drug and drug uptake as high as 512 mg/g.

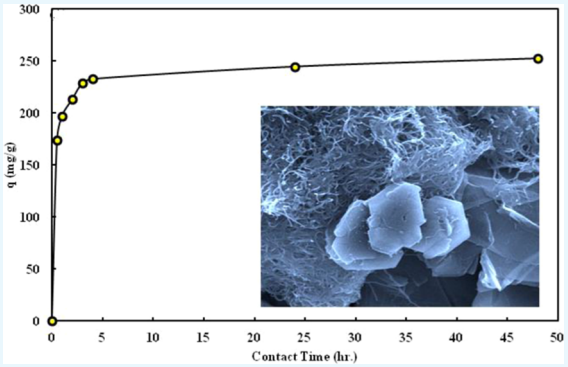

INTRODUCTION

In recent years, the presence of pharmaceutical medicines and drugs in sewage, wastewaters, and domestic waters has been found to be responsible for huge ecotoxicological effects on human health in different countries.[1] The toxic side effects of pharmaceuticals in water resources are extremely dangerous and have serious consequences on human health, animals, and plants. Several studies have described the harmful effects of pharmaceuticals on the aquatic environment and their adverse ability to influence sexual functions and endocrine activity of humans and animals.[2,3] Nano- or microscale concentrations of drugs were not previously considered harmful, but it has become tremendously important to carefully monitor their concentrations in aquatic environments.[4,5] Growing drug concentrations, especially antibiotic drugs, in sewage treatment effluents, wastewaters, and drinking waters are mainly due to poorly metabolized drugs in the human body secreted through human urine or dislodged feces routes.[6] The increased annual consumption of pharmaceutical drugs has led to an increase in their concentration in wastewaters, which has reached 15 g per year per person, and it is expected to increase in the future to 50−150 g.[7] If the concentration of such drugs exceeds the shelf concentration, they can become toxic to humans, animals, and plants. Therefore, drug concentration in wastewaters must be measured to assess the ecotoxicity on a daily basis.[8] Latest statistics indicate that there are more than 3700 approved pharmaceutical drugs in the world.[9] This huge number of drugs indicates how difficult it is to treat their toxicity efficiently and how complicated their removal techniques are in wastewaters.

Bacteria can frequently generate resistance against antibiotic drugs in the human body called antimicrobial resistance (AMR). The generated resistance occurs through mutations in their genes or by acquisition of foreign DNA coding through horizontal gene transfer, and the bacteria can survive, and even grow, in the presence of antibiotic drugs, leading to a condition under which the drugs become noneffective on the patient, which aggravates with time and, at the end, may lead to

Received: October 29, 2019
Accepted: January 29, 2020
Published: February 26, 2020

https://dx.doi.org/10.1021/acsomega.9b03636
ACS Omega 2020, 5, 4457−4468

death.[10−13] The most recent global statistics has declared 700,000 deaths in 2016 related to AMR and noneffective drugs,[14] and the human mortality rate will reach 10 million per year by the year 2050.[15] Antibiotics in the aquatic environment were considered responsible for human endocrine disruption.[16] Moreover, pharmaceutical drugs caused a decrease in the number of fish through increasing intersex and reducing fecundity[17] and an increase in mortality rates of birds, especially vultures.[18] Such horrifying information if not treated carefully can threaten the survival of humans, animals, and plants on the globe. Therefore, innovative eradication strategies must be developed to remove drugs entirely from wastewaters, and new government regulations must be established and enforced to eradicate pharmaceutical drugs from wastewaters. The ciprofloxacin antibiotic is a widely used antibiotic that targets Gram-negative and Gram-positive bacteria.[19] According to the U.S. government data, there were more than 7 million medical prescriptions for ciprofloxacin in 2019.[20] Different countries have confirmed the presence of ciprofloxacin in their municipal wastewaters and drinking water.[21−25] The risk quotient (RQ) scale for ciprofloxacin was identified as a high risk to the environment.[23] Desbiolles found that ciprofloxacin is one of the most hazardous pharmaceuticals in 75% of Mediterranean wastewater samples.[8] Due to the chemical structure of ciprofloxacin, it is considered a genotoxic compound, so it needs close monitoring and treatment.[22] Zhang conducted a study on the relation between antibiotics and heavy metals, and the results showed that the interaction of the antibiotic, ciprofloxacin, with a group of heavy metals, copper, zinc, and cadmium, via coordination sites gave rise to complexes that are more toxic than the interacting compounds[26] (Figure 1).

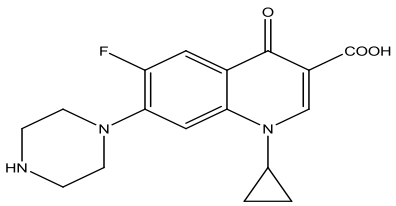

Figure 1. Ciprofloxacin drug.

Versatile techniques have been employed to remove pharmaceutical drugs from wastewater, such as the conventional activated sludge process,[27] anaerobic sludge digestion,[28] biosorption,[29] oxidation,[30] reverse osmosis,[31] removal using activated carbon,[32] photobioreactors, and[16] nanotechnology.[33] Carbon nanotubes (CNTs) have two forms: single-walled and multiwalled carbon nanotubes arranged in a hexagonal shape with outer diameters of 4−30 nm, inner diameters of up to 0.4 μm, length of around 1 μm, and a high adsorption surface area of over 1000 m^2/g.[34] Carbon nanotubes (CNTs) have high adsorption capacity due to their porous nature[35,36] and are used to remove pharmaceutical products from wastewater.[37,38] Graphene consists of a two-dimensional carbon layer that makes graphene the thinnest material ever and has a specific surface area of about 2630 m^2/g; many scientific disciplines are concerned with the research on graphene, such as physics, materials science, chemistry, and biology.[39] Recently, oxidized graphene (GO) nanocomposites have been used to eliminate pharmaceutical and personal-care products.[40−45] GO has a higher ability to adsorb polar materials than nonpolar ones; the reason behind this is the strong interactions between polar materials and polar functional groups on GO.[46]

In this work, we synthesized new nanohybrid materials composed of graphene oxide (GO) and oxidized carbon nanotubes (O-CNTs) to fully eliminate the ciprofloxacin drug from aqueous solutions. The ultimate eradication strategy was established toward fighting against the induced antimicrobial resistance (AMR) formed thereafter. The innovative nanohybrid material was characterized by different techniques. Optimum conditions, dynamics, and thermodynamics for the eradication of drugs were also investigated.

EXPERIMENTAL SECTION

Materials. Carbon nanotubes were purchased from Nanocyl NC7000, graphene was purchased from Sigma-Aldrich, and the ciprofloxacin drug (>99%) was gifted by a local pharmaceutical company. Other reagents were of analytical grade and were used as received. Tween 80, purchased from BBC chemicals, was used as a dispersion surfactant, and its micellar average molar mass was 79 000. Concentrated acids used in the study were HCl (Scharlau), H_2SO_4 (Riedel-de Haën), HNO_3 (BBC Chemicals), and H_3PO_4 (Riedel-de Haën). H_2O_2 was obtained from Merck.

Investigation Techniques. *Fourier Transform Infrared (FTIR) Spectroscopy.* A Bruker FTIR spectrometer was used to investigate functional groups after the oxidation process of graphene and multiwalled carbon nanotubes (CNTs). Spectra were recorded in the range of 4000−400 cm^{-1} using KBr pellets. Thermogravimetric analysis (TGA), with a Netzsch Proteus thermogravimetric analyzer, was performed to study the thermal stability of GO and multiwalled CNTs before and after the oxidation processes. The samples were heated from ambient temperature to 900 °C at a heating rate of 10 °C/min under a stream of inert N_2 gas. The derivative thermogravimetry (DTG) technique was used to determine the decomposition temperature of the samples. Scanning electron microscopy [SEM; Inspect F50 scanning electron microscope equipped with a high-resolution Schottky field emission gun (FEG), high-vacuum Bruker energy-dispersive spectrometry (EDS) microanalyzer, and XFlash silicon drift detector (SDD)] was used to study the topological changes of graphene and multiwalled CNTs before and after the oxidation processes. The samples were sputtered by gold ions before being imaged. All images were tuned and resolved by software programs of the instrument. UV−vis spectrophotometry (Hach Lange DR5000 UV−vis spectrophotometer) was used to detect ciprofloxacin concentrations at different time intervals. The samples were scanned in the range of 200−800 nm and the maximum wavelength (λ_{max}) was selected as 275 nm. The calibration curve for the ciprofloxacin drug was established, and the drug concentration was monitored accordingly. For X-ray diffraction (XRD) studies, a Rigaku X-ray diffractometer (Ultima IV; 1 and 5 mm) with Cu Kα radiation was used. An accelerating tube voltage of 40 kV and a tube current of 40 mA were used to study the crystalline structure of graphene and multiwalled CNTs before and after the oxidation process. The scanning rate was 2°/min in the angle range from 5 to 60°.

Preparation of GO. Graphene (225 mg) was mixed with 30 mL of a mixture of sulfuric acid (H_2SO_4) and phosphoric acid (H_3PO_4) (9:1 ratio) under continuous stirring for 6 h according to Hummers' method.[47] Later on, 1.32 g of potassium permanganate ($KMnO_4$) was added, and 675 μL

https://dx.doi.org/10.1021/acsomega.9b03636
ACS Omega 2020, 5, 4457−4468

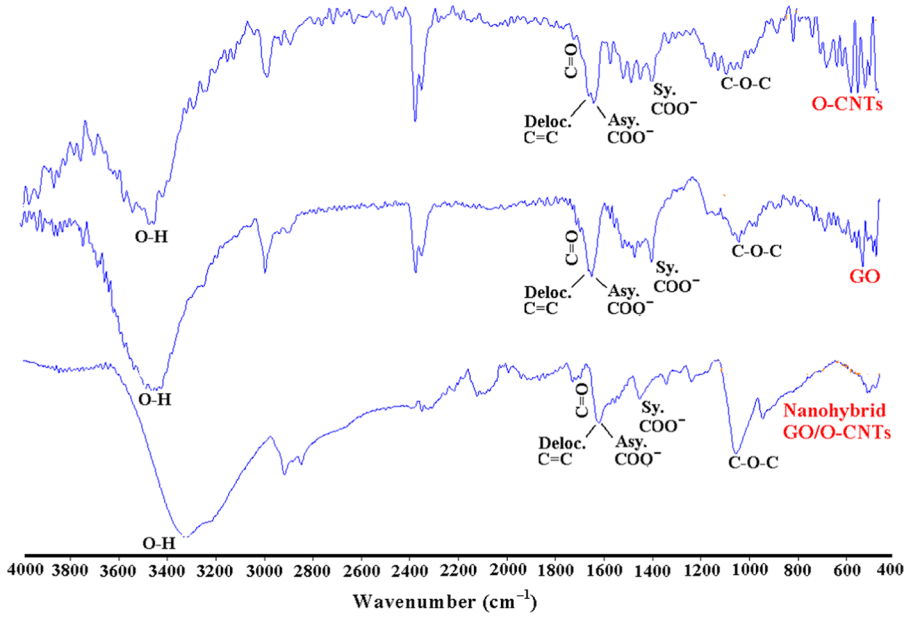

Figure 2. FTIR transmittance spectra of oxidized carbon nanotubes (O-CNTs), graphene oxide (GO), and nanohybrid GO/O-CNTs.

of hydrogen peroxide (H_2O_2) was slowly dropped to remove unreacted $KMNO_4$. Diluted hydrochloric acid (HCl) was added, and the solution was centrifuged and decanted. Eventually, the final product was washed with a concentrated HCl:H_2O solution (1:3 ratio) and dried.[48]

Preparation of O-CNTs. Briefly, 2.0 g of multiwalled carbon nanotubes was placed in a dried 50 mL round-bottom flask equipped with a condenser and 30 mL of 9.0 M HNO_3 solution was slowly added. The mixture was refluxed at 75 °C for 24 h, and after completion, the oxidized CNTs were filtered and the suspended O-CNTs particles were collected by centrifugation. The oxidized CNTs (O-CNTs) were purified from nitric acid traces by continuous washing with distilled water several times until the pH of the filtrate solution became neutral. The O-CNT sample was dried at room temperature and stored until used.[49]

Synthesis of Nanohybrid GO/O-CNTs. Graphene oxide (GO, 0.5 g) was dispersed in 150 mL of 2.5% Tween 80 surfactant solution (w/w) under continuous stirring at 70 °C for 2 h to make a water-dispersed graphene oxide (GO) solution. Similarly, in a separate tube, 0.5 g of oxidized carbon nanotubes (O-CNTs) was dispersed in 150 mL of 2.5% Tween 80 surfactant solution at 70 °C to make a water-dispersed CNT solution.[50] The dispersed solutions of GO and O-CNTs were slowly mixed and added dropwise into a $CaCl_2$ solution to make 2% $CaCl_2$ concentration under stirring (100 rpm). For complete nucleation of the nanohybrid sample, the mixture was left stirring overnight at ambient temperature. The final nanohybrid product was collected by centrifugation, and the nanohybrid GO/O-CNT materials were dried and stored until used elsewhere.

Ultimate Drug Eradication. The nanohybrid GO/O-CNT material was placed in ciprofloxacin drug solutions of various concentrations and shaken in a Memmert shaker for various periods of time. After completion, the sample was centrifuged at 4000 rpm for 15 min, and the supernatant was decanted. The ciprofloxacin drug uptake by the nanohybrid GO/O-CNTs was calculated from the following relation

$$q_e = \frac{(C_0 - C_e)V}{w} \quad (1)$$

where q_e is the equilibrium drug uptake (in mg/g), C_0 is the initial concentration of the drug (in mg/L), C_e is the equilibrium drug concentration (in mg/L), V is the volume of the solution (in L), and w is the mass of the nanohybrid material (in g).

Batch adsorption experiments were conducted to investigate and optimize the adsorption conditions. For optimization of contact time, 1 mg of nanohybrid was added into ciprofloxacin solutions having a concentration of 15 ppm for time intervals from 0.5 to 48 h. The following parameters were kept fixed during experiments: pH = 6.0, solution volume = 30 mL, temperature = 17 °C, GO/O-CNT ratio = 1/1, and %$CaCl_2$= 2.0%. For optimization of the mass of nanohybrid, different masses in the range of 1−5 mg were used for the eradication process at fixed pH = 6.0, solution volume = 30 mL, contact time = 4 h, temperature = 17 °C, GO/O-CNT ratio = 1/1, and %$CaCl_2$= 2.0%. For optimization of temperature, batch adsorption experiments were carried out in the 290−303 K range at fixed pH = 6.0, solution volume = 30 mL, contact time = 4 h, nanohybrid mass = 1 mg, GO/O-CNT ratio = 1/1, and %$CaCl_2$= 2.0%. For optimization of solution pH, different pH values in the range 2−11 were used at fixed contact time = 4 h, solution volume = 30 mL, temperature = 17 °C, nanohybrid mass = 1 mg, GO/O-CNT ratio = 1/1, and %$CaCl_2$= 2.0%. For optimization of the $CaCl_2$ cross-linker, different concentrations were used (0.5, 2, and 4%) at fixed pH = 6.0, solution volume = 30 ml, contact time = 4 h, nanohybrid mass = 1 mg, temperature = 17 °C, and GO/O-CNT ratio = 1/1. Finally, for optimization of the GO/O-CNT ratio, different ratios of GO to O-CNTs were used (1/2, 1/3, 1/4, 1/1, 2/1, 3/1, and 4/1) at fixed pH = 6.0, solution volume = 30 mL, contact time = 4 h, nanohybrid mass = 1 mg, temperature = 17 °C, and %$CaCl_2$ = 2.0%.

Desorption Process. Desorption of adsorbed drugs on the surface of the adsorbent is a particularly important step toward the reuse of the adsorbent over and over in the drug eradication process. This permits the reuse of nanohybrid GO/

https://dx.doi.org/10.1021/acsomega.9b03636
ACS Omega 2020, 5, 4457−4468

O-CNTs several times to remove the ciprofloxacin drug from aqueous solutions. For this purpose, 500 mg of nanohybrid GO/O-CNTs was immersed in 500 mL of 0.4 M NaOH solution and allowed to mix overnight at ambient temperature; then, the nanohybrid was decanted and washed several times with distilled water to remove traces of the ciprofloxacin drug. Nanohybrid GO/O-CNTs was dried and stored until reused again.[51]

RESULTS AND DISCUSSION

Structural Composition. Carboxylic-functionalized graphene and carbon nanotubes were observed and identified through the Fourier transform infrared (FTIR) technique. Figure 2 shows the FTIR spectra of graphene oxide (GO), oxidized carbon nanotubes (O-CNTs), and nanohybrid GO/O-CNTs. In addition, Table 1 illustrates the characteristic vibrational assignments and their corresponding wavenumbers. In graphene oxide, a broad peak of the hydroxyl (OH) group at 3447 cm^{-1}, peaks of asymmetric and symmetric carboxylate (COO^-) groups at 1632 and 1385 cm^{-1}, carbonyl (C═O) group at 1711 cm^{-1}, and epoxy groups (COC) at 1031 cm^{-1} proved the successful oxidation process of graphene. Moreover, the peak of delocalized C═C stretching at 1645 cm^{-1} proved the accomplished oxidation process without complete destruction of the graphene carbon skeleton. This is a very critical step because in some oxidation processes, a collapse of the carbon skeleton of nanoparticles may occur. Likewise, in oxidized carbon nanotubes (O-CNTs), peaks of dense hydroxyl (OH) groups at 3451 cm^{-1}, respective asymmetric and symmetric carboxylate (COO^-) groups at 1625 and 1385 cm^{-1}, carbonyl (C═O) group at 1709 cm^{-1} and epoxy groups (COC) at 1080 cm^{-1} demonstrated the complete oxidation process of CNTs. In addition, the appearance of a dense delocalized C═C peak at 1649 cm^{-1} endorsed the retained carbon skeleton of CNTs during the oxidation process. Nanohybrid GO/O-CNTs equally shows the functional groups of GO and O-CNTs. Cross-linking of carboxyl groups (COO^-) of GO and O-CNTs via Ca^{2+} ions was established by a decrease in the intensity of asymmetric and symmetric COO^- peaks and an instantaneous increase in the intensity of the carbonyl (C═O) peak (Figure 2).

Thermal Stability. The thermal stability of compounds was measured by thermogravimetric analysis (TGA) and its derivative thermogravimetry (DTG) technique evaluated the ability of the sample to withstand elevated temperatures until it decomposed. The midpoint peak of DTG thermograms shows the decomposition temperature and displays the thermal stability of samples. Figure 3A,B shows the TGA and DTG thermograms of graphene oxide (GO), oxidized carbon nanotubes (O-CNTs), and nanohybrid GO/O-CNTs, respectively. Two decomposition temperatures of GO are observed at 225 and 680 °C, respectively. The peak below 100 °C is attributed to adsorbed water on the surface of GO. The peak at 225 °C is assigned to pyrolysis of labile oxygen functional groups, such as CO_2, CO, gases, and steam.[52−54] The peak at 680 °C is due to the destruction of the carbon skeleton of graphene oxide.[55] In contrast, oxidized carbon nanotubes display no degradation temperature up to 900 °C, as observed in the DTG thermogram (Figure 3B), which confirms the absence of disordered carbon responsible for degradation and the presence of a tough carbon skeleton during the oxidation process.[56] It may also indicate that the oxidation process occurs on the external surface of carbon nanotubes, as evidenced by FTIR spectra. On the other hand, nanohybrid GO/O-CNTs displays the onset of decomposition at 250 °C and its end at 450 °C with the midpoint peak of decomposition at 350 °C for different GO:O-CNTs ratios (Figure 3B). During the cross-linking of carboxylate groups (COO^-) of GO with the carboxylate groups (COO^-) of O-CNTs, the decomposition temperature of the labile oxygen groups in GO increased from 225 to 350 °C, and moreover, the peak at 680 °C disappeared in the nanohybrid samples. This demonstrated that the thermal stability of GO sheets increased due to cross-linking with O-CNT cylinders at all GO:O-CNTs ratios of the nanohybrid.

Table 1. Characteristic FTIR Vibrational Assignments with Their Wavenumbers for Graphene Oxide (GO), Oxidized Carbon Nanotubes (O-CNTs), and Nanohybrid GO/O-CNTs

nanomaterial	wavenumber (cm^{-1})	vibrational assignments
graphene oxide (GO)	3447	O−H stretching
	3042	aromatic C−H stretching
	2979	asymmetric C−H stretching
	2886	symmetric C−H stretching
	1711	C═O stretching
	1645	conjugated C═C stretching
	1632	asymmetric COO^- stretching
	1385	symmetric COO^- stretching
	1031	COC stretching
oxidized carbon nanotubes (O-CNTs)	3451	O−H stretching
	3031	aromatic C−H stretching
	2975	asymmetric C−H stretching
	2882	symmetric C−H stretching
	1709	C═O stretching
	1649	conjugated C═C stretching
	1625	asymmetric COO^- stretching
	1385	symmetric COO^- stretching
	1080	COC stretching
nanohybrid GO/O-CNTs	3342	O−H stretching
	3005	aromatic C−H stretching
	2918	asymmetric C−H stretching
	2851	symmetric C−H stretching
	1734	C═O stretching
	1644	conjugated C═C stretching
	1632	asymmetric COO^- stretching
	1346	symmetric COO^- stretching
	1067	COC stretching

Crystal Structure and Interlayer Spacings. The crystal structure of the new nanohybrid materials was identified from X-ray diffraction (XRD) patterns. The spacing between the

https://dx.doi.org/10.1021/acsomega.9b03636
ACS Omega 2020, 5, 4457−4468

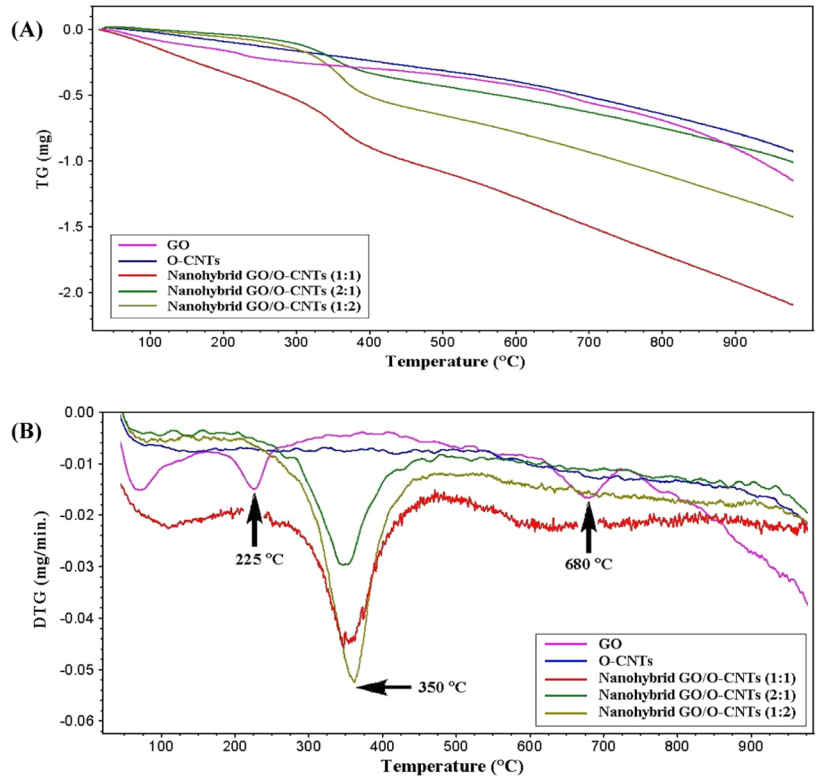

Figure 3. (A) TG and (B) DTG thermograms of graphene oxide (GO), oxidized carbon nanotubes (O-CNTs), and nanohybrid GO/O-CNTs (1:1, 2:1, and 1:2 ratios).

crystal planes of graphene, graphene oxide, carbon nanotubes (CNTs), oxidized carbon nanotubes (O-CNTs), and nanohybrid GO/O-CNTs was calculated using Bragg's equation as follows

$$n\lambda = 2d \sin\theta \quad (2)$$

where n is chosen as 1, λ is the X-ray wavelength taken as 1.5406 Å using Cu Kα radiation, θ is Bragg's angle, and d is the interlayer spacing between crystal planes. A distinctive diffraction peak (002) of graphene at 26.14° with an interlayer spacing of 3.4 Å corresponds to hexagonal crystalline graphite[57] between graphene nanosheets, as illustrated in Figure 4. However, GO displays two lower intensity peaks at 11.55 and 23.00° with interlayer spacings of 7.7 and 3.9 Å, which match with hexagonal crystalline graphite. The interlayer spacing between crystalline planes alters with the degree of oxidation; the higher level of oxidation of GO yields several functional groups on the surface of GO and, subsequently, larger interlayer spacings between GO nanosheets.[58,59] The appearance of broad peaks with wider interlayer spacing values indicates the formation of irregular disordered structures due to labile oxygen functional groups on the surface of GO nanosheets. Moreover, CNTs have two peaks at 25.66 and 43.38°, representing the (002) hexagonal graphite and the (100) diffraction of graphite.[60] Likewise, O-CNTs have the same two peaks appearing in CNTs with higher intensity values. The increase in the intensity of peaks for O-CNTs provides evidence for the successful oxidation process, and the identical peak angles for O-CNTs and CNTs prove that the crystal structure is not affected by the oxidation process.[50] Nanohybrid GO/O-CNTs shows two peaks at 24.7 and 42.9°, regardless of the ratio of GO to O-CNTs. These diffraction peaks correlate with the (002) and (100) crystal planes.[61] Peak broadening of nanohybrid GO/O-CNTs is attributed to the crystalline defects and disordered structures and to the exfoliation process that occurs during the formation of nanohybrids.[59,62]

Topology. The topological structure and morphological changes of nanoscale adsorbents were monitored using the scanning electron microscopy (SEM) technique. Graphene shows two-dimensional nanosheets stacked above each other with 1−2 μm flake size and versatile flake thickness (Figure 5A). However, graphene oxide shows 2D nanosheets but with exfoliated flakes. The exfoliation occurs due to crystalline defects that appear on the nanohybrid surface during the oxidation process (Figure 5B). The thin GO flakes hold hydroxyl, carboxyl, and epoxy functional groups on their inner and outer surfaces. On the other hand, oxidized multiwalled carbon nanotubes (O-CNTs) show cylindrical-shaped nanotubes that hold labile oxygen functional groups (i.e., hydroxyl, carbonyl, carboxyl, and epoxy) on their surfaces (Figure 5C). When cylindrical O-CNTs are cross-linked with sheets of GO via Ca^{2+} ions, the carboxyl groups of GO and O-CNTs bind through the cross-linking agent (Ca^{2+}). The threads of O-CNTs settle down on the surface of the GO sheets, as demonstrated in Figures 5D,E. Likewise, at the 1:4 ratio, a higher content of threads of O-CNTs are cross-linked with GO nanosheets (Figure 5F).

Optimum Parameters for Ultimate Eradication. Versatile parameters and conditions were designed to inspect the optimum conditions for ultimate eradication of drugs from aqueous solutions. For this purpose, batch adsorption experiments were processed, and the parameters were investigated in the following order: contact time, nanohybrid mass, temperature, solution pH, percent of cross-linking agent

https://dx.doi.org/10.1021/acsomega.9b03636
ACS Omega 2020, 5, 4457−4468

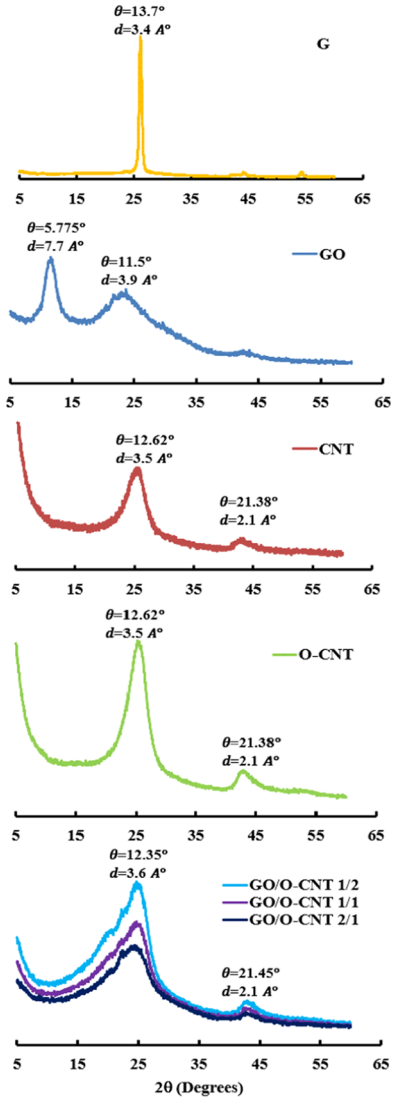

Figure 4. XRD patterns with diffraction angle (θ) and interlayer spacing (d) values of graphene (G), graphene oxide (GO), carbon nanotubes (CNTs), oxidized carbon nanotubes (O-CNTs), and nanohybrid GO/O-CNTs (1:2, 1:1, and 2:1 ratios).

($\%CaCl_2$), and the ratio of GO to O-CNTs in the nanohybrid structure.

Contact Time, Nanohybrid Mass, and Solution Temperature. The influence of contact time, nanohybrid mass, and solution temperature was investigated for ultimate eradication of the ciprofloxacin drug from aqueous solutions (Figure 6A–C). For this purpose, different contact times of drug with the nanohybrid adsorbent were selected. Clearly, drug uptake increased exponentially in the first 4 h until an equilibrium was established. Quick drug uptake occurred within the first 4 h, followed by slow equilibrium drug uptake. Quick drug uptake occurred due to the existence of many vacant sites for adsorption with no internal resistance for diffusion.[63] Beyond 4 h, the slow drug uptake was due to slow saturated diffusion to less accessible sites.[64,65] Therefore, 4 h was selected as the optimum time for equilibrium (Figure 6A). As shown in Figure 6B, variable nanohybrid masses in the range of 1–5 mg were used for the eradication process; the 1 mg sample removed almost twice the amount of drug compared with the 2 mg sample. Apparently, with a higher nanohybrid mass, chains of GO and O-CNTs established intermolecular interactions and accumulated above each other, thus covering many of the active sites, which inhibited drug uptake. In addition, for temperature optimization, batch adsorption experiments were carried out in the 290–303 K range. Obviously, as the temperature increased, the drug uptake decreased. This was due to the increased kinetic energy of the surface of nanohybrid GO/O-CNTs and the ciprofloxacin molecules in solution, which depleted the drug uptake and minimized the adsorbent–adsorbate interactions.[66]

Solution pH, %Cross-linking Agent, and GO/O-CNT Ratio. The influence of solution pH on the drug uptake was investigated in the range pH = 2–11 (Figure 6D). Drug uptake shows a distribution curve over the pH range with the maximum uptake at pH = 6.0. Adsorption of ciprofloxacin on the surface of nanohybrid GO/O-CNTs occurs via H-bonding and/or $\pi-\pi$ stacking interactions. Furthermore, the ciprofloxacin drug has two pK_a values of 5.9 and 8.9.[67] At pH < 5.9, ciprofloxacin is protonated and holds positive charges, and at pH > 8.9, ciprofloxacin is deprotonated and holds negative charges. In both cases, the presence of charges weakens and diminishes H-bonding interactions between ciprofloxacin molecules and the surface of nanohybrid GO/O-CNTs, which lowers the drug uptake. In the pH 6–7 range, the ciprofloxacin drug becomes chargeless and the strongest H-bonding with the adsorbent surface occurs; hence, the maximum drug uptake takes place.

The effect of concentration of the cross-linking agent ($\%CaCl_2$) in the nanohybrid and its relation to drug uptake is investigated in Figure 6E. Clearly, the increase in concentration of $CaCl_2$ in the nanohybrid backbone structure leads to a large decrease in the drug uptake due to the formation of small-sized nanochannels in the GO networks that eliminate sorbed water[68] and, certainly, prevent larger molecules, such as the ciprofloxacin drug, from being adsorbed on the inner layers of the nanohybrid adsorbent. Furthermore, the variable ratios of GO to O-CNTs in the nanohybrid give rise to different microstructures that show versatile drug uptake, as described in Figure 6F. The maximum drug uptake of 512 mg/g was obtained using 1:4 ratio of GO to O-CNTs. Apparently, the 1:1 ratio shows the lowest drug uptake due to cooperatively strengthened $OH^{\cdots}O{=}C$ hydrogen bonds that align and assemble O-CNT cylinders on GO sheets and hence decrease their surface area for drug uptake,[69] as observed in the SEM image (Figure 5F).

Ultimate Eradication of Ciprofloxacin from Aqueous Solutions. The ultimate eradication of the drug is an extremely essential part in this study, not only due to the importance of drug eradication from aqueous solutions but also due to the significance of fighting against the generated antimicrobial resistance (AMR) in the human body. The generated AMR will ultimately lead to drug deactivation in the human body and to massive number of deaths associated with generated AMR.[14] To investigate the entire eradication process of the drug, different initial concentrations of the drug (5–15 ppm) and different nanohybrid adsorbent masses (1–5 mg) were used (Figure 7A). The removal efficiency (in %) was calculated with respect to the initial concentration of the drug under optimum conditions. Obviously, a high removal efficiency was obtained using a high nanohybrid mass and low initial concentration of the drug. The maximum efficiency for the entire removal process was 99.2% at 5 ppm of the drug using 5 mg of the nanohybrid adsorbent.

https://dx.doi.org/10.1021/acsomega.9b03636
ACS Omega 2020, 5, 4457–4468

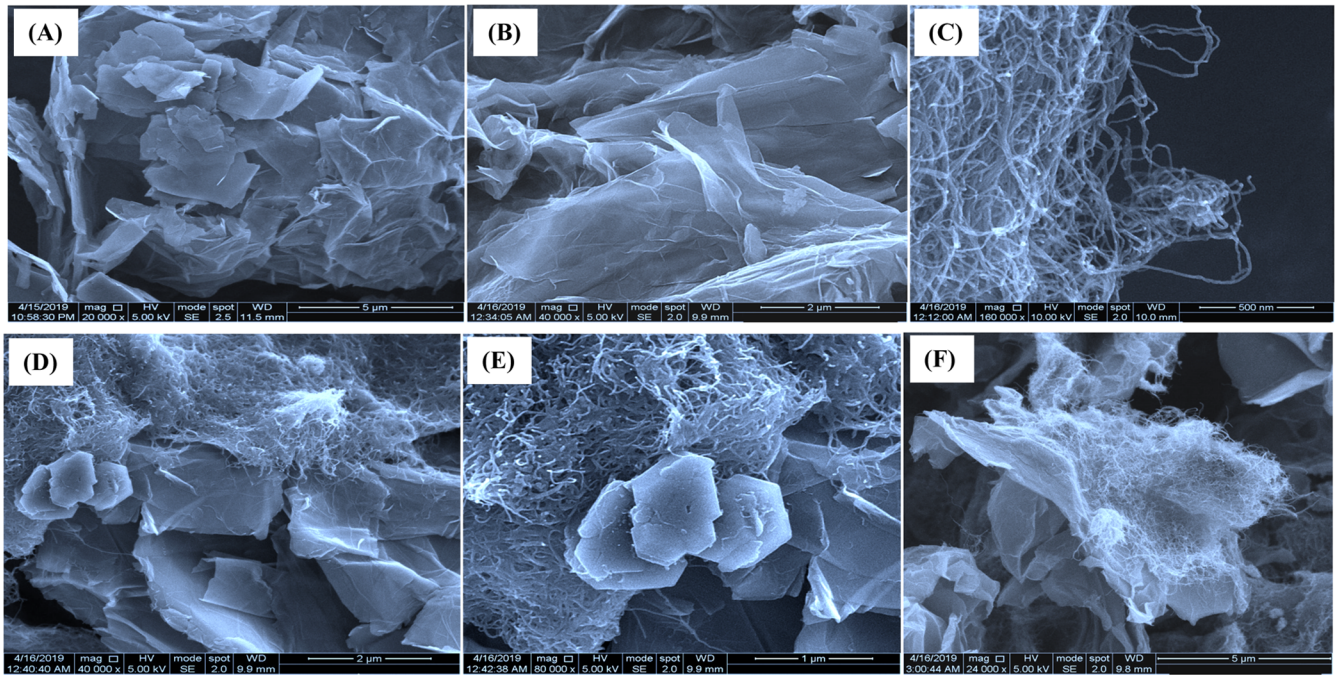

Figure 5. Scanning electron microscopy images of (A) graphene, (B) graphene oxide (GO), (C) oxidized carbon nanotubes (O-CNTs), (D, E) nanohybrid GO/O-CNTs (1:1), and (F) nanohybrid GO/O-CNTs (1:4).

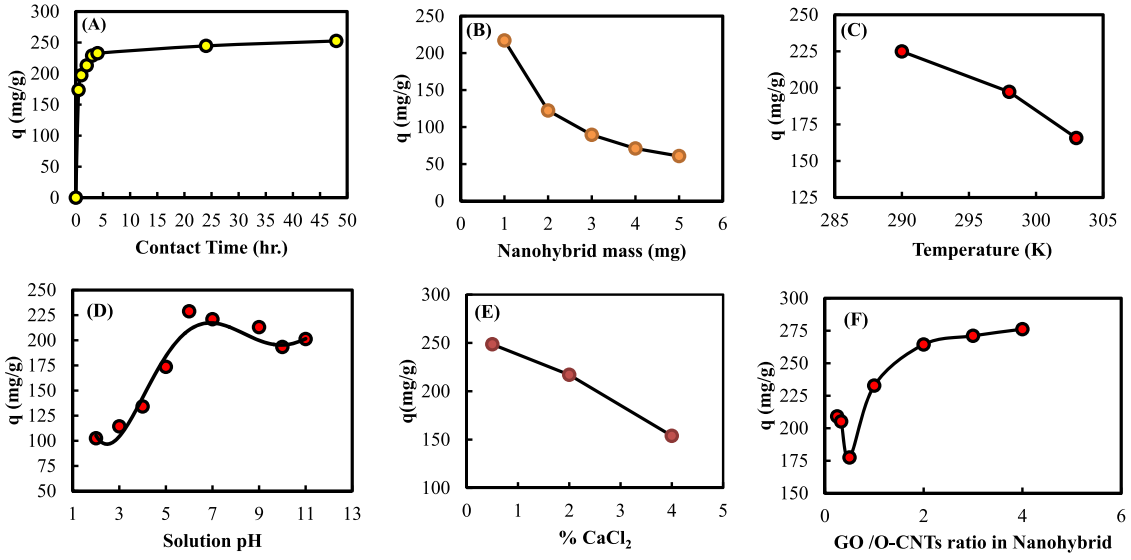

Figure 6. Optimum conditions for adsorption of the ciprofloxacin drug on the surface of nanohybrid GO/O-CNTs: (A) Contact time (pH = 6.0, solution volume = 30 mL, nanohybrid mass = 1 mg, temperature = 17 °C, GO/O-CNT ratio = 1/1, %$CaCl_2$= 2.0%), (B) nanohybrid mass (pH = 6.0, solution volume = 30 mL, contact time = 4 h, temperature = 17 °C, GO/O-CNT ratio = 1/1, %$CaCl_2$= 2.0%), (C) temperature (pH = 6.0, solution volume = 30 mL, contact time = 4 h, nanohybrid mass = 1 mg, GO/O-CNT ratio = 1/1, %$CaCl_2$= 2.0%), (D) solution pH (contact time = 4 h, solution volume = 30 mL, temperature = 17 °C, nanohybrid mass = 1 mg, GO/O-CNT ratio = 1/1, %$CaCl_2$= 2.0%), (E) %cross-linker (pH = 6.0, solution volume = 30 ml, contact time = 4 h, nanohybrid mass = 1 mg, temperature: 17 °C, GO/O-CNT ratio = 1/1), and (F) GO/O-CNT ratio in the hybrid (pH = 6.0, solution volume = 30 ml, contact time = 4 h, nanohybrid mass = 1 mg, temperature = 17 °C, %$CaCl_2$ = 2.0%).

Regeneration of Nanohybrid GO/O-CNTs. Batch adsorption experiments on the regenerated adsorbent have proved the possible regeneration of nanohybrid GO/O-CNTs for multiple adsorption−desorption processes. The average removal efficiency of three tested samples of the regenerated adsorbent was reduced only by 2.0% compared to the original fresh adsorbent. This also reflected the high structural stability of the nanohybrid adsorbent against continuous washing with basic aqueous solutions.

Ciprofloxacin Eradication Dynamics. Versatile models for drug eradication dynamics were investigated, and the drug uptake proved to be a pseudo-second-order model, with the correlation coefficient value (R^2) exceeding 0.99. The second-order model is as follows

$$\frac{t}{q_t} = \frac{1}{k_2 q_e^{\,2}} + \frac{t}{q_e} \quad (3)$$

https://dx.doi.org/10.1021/acsomega.9b03636
ACS Omega 2020, 5, 4457−4468

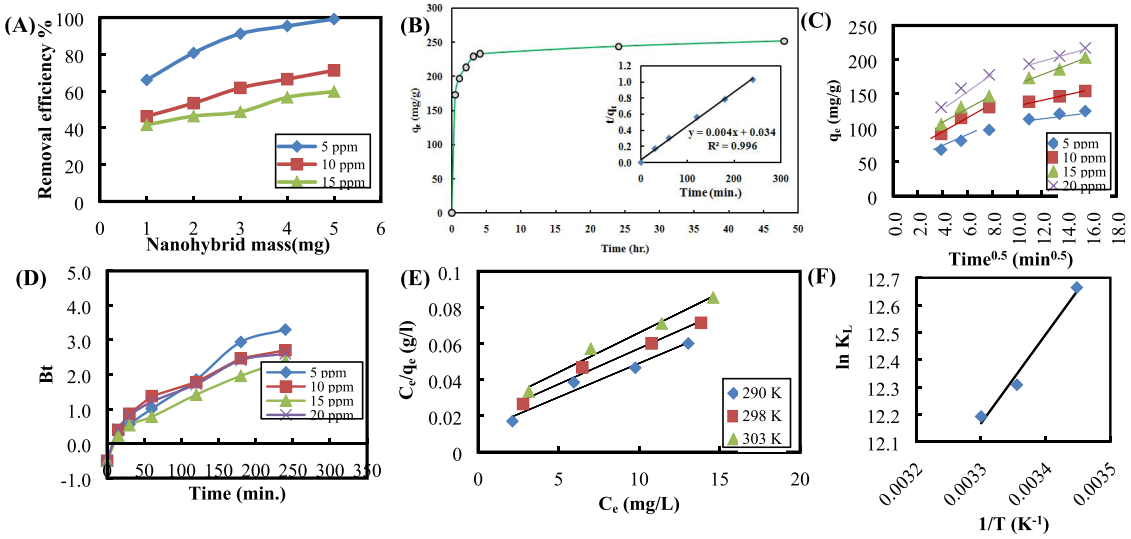

Figure 7. (A) Effect of adsorbent mass on the removal efficiency of ciprofloxacin on GO/O-CNTs at different initial concentrations (pH: 6.0, volume: 30 ml, time: 4 h, temperature: 17 °C, GO/O-CNT ratio: 1/1, %$CaCl_2$: 2.0%), (B) dynamic change of drug uptake (q_e) versus time (t) and pseudo-second-order plot (inner curve), (C) intraparticle diffusion dynamics curves for drug removal by nanohybrid GO/O-CNTs from aqueous solution, (D) Boyd plot for removal of various concentrations of the drug by nanohybrid GO/O-CNTs, (E) Langmuir adsorption isotherms for drug removal at elevated temperatures, and (F) ln K_L versus reciprocal temperature ($1/T$) curve for determination of thermodynamic parameters.

where q_e is the equilibrium drug uptake (in mg/g), q_t is the drug uptake at time t (in mg/g), k_2 is the rate constant of drug uptake (in g/mg min), and t is the time (in min).[70] By plotting t/q_t against time t, the equilibrium drug uptake (q_e) and the rate constant of removal (k_2) were determined (Table 2). The

Table 2. Kinetic Rate Constants for Ciprofloxacin Removal Using a Pseudo-Second-Order Kinetic Model

$q_{e,exp}$ (mg/g)	k_2 (g/mg min)	$q_{e,cal}$ (mg/g)	R^2
232.8	4.71×10^{-4}	250.0	0.996

calculated equilibrium drug uptake (q_e) was 250 mg/g, and the rate constant of removal (k_2) was 4.71×10^{-4} g/mg min with a correlation coefficient (R^2) of 0.996 (Figure 7B).

Furthermore, the mechanism of drug adsorption was validated using the intraparticle diffusion model.[71]

$$q_t = k_p t^{1/2} + C \quad (4)$$

where k_p is the intraparticle diffusion constant (in mg/g $min^{0.5}$), and C is the adsorption constant (in mg/g). Plots of q_t versus $t^{1/2}$ in Figure 7C show two different straight lines, which suggest an intraparticle diffusion mechanism and prove that many steps control the overall drug uptake process.[72] The steps include quick external pore diffusion (film diffusion) followed by slow sorption on the internal pore surface of the nanohybrid adsorbent (pore diffusion).[73]

The Boyd model[74] was used to determine the rate-controlling step of the adsorption process[75] as follows

$$F = \frac{q_t}{q_e} \quad (5)$$

$$\mathrm{Bt} = -0.4977 - \ln(1 - F) \quad (6)$$

where F is the equilibrium fractional attainment calculated from eq 5, B is the time constant (in 1/min), and Bt is calculated from eq 6. According to the Boyd model, the plot of

Table 3. Adsorption Isotherm Parameters for Ciprofloxacin Drug Removal

		temperature (K)		
isotherm	parameters	290	298	303
Langmuir	q_{max} (mg/g)	270.3	253.2	227.3
	K_L (L/mg)	0.316	0.222	0.197
	R^2	0.968	0.984	0.982
Freundlich	$1/n$	0.322	0.391	0.403
	K_F ($(mg^{(1-1/n)}\ L^{(1/n)})/g$)	94.63	69.06	58.28
	R^2	0.942	0.990	0.986
Temkin	K_T (L/mg)	4.25	2.14	1.83
	b_T	45.07	44.08	48.92
	B_T (J/mol)	53.50	56.2	51.49
	R^2	0.915	0.974	0.970
D–R	q_{max} (mg/g)	379.7	387.2	349.0
	B (mol^2/kJ^2)	0.01	0.0063	0.0061
	E (kJ/mol)	7.07	12.60	12.80
	R^2	0.930	0.980	0.979

https://dx.doi.org/10.1021/acsomega.9b03636
ACS Omega 2020, 5, 4457−4468

Bt versus t that forms a straight line and passes through the origin is direct proof that the adsorption process is controlled by the intraparticle diffusion mechanism. Otherwise, the film diffusion step is the rate-determining step. Our results show that the straight lines of all drug uptake processes do not pass through the origin, which suggests that the drug uptake process is controlled by rapid external pore diffusion (the film diffusion step)[72,76]

Ciprofloxacin Eradication Isotherms. Isothermal determination of the amount of drug adsorbed on the surface of an adsorbent can be best described by adsorption isotherms. In general, the number of vacant active sites and the size of pores on the surface of the adsorbent play major role in the determination of the amount of drug adsorbed. Four adsorption models were applied to the adsorption of the ciprofloxacin drug on the surface of the nanohybrid GO/O-CNT system: Langmuir, Freundlich, Temkin, and Dubinin–Radushkevich isotherms, respectively. The adsorption isotherms exhibited linear curves with the highest correlation coefficients (R^2) of 0.97–0.98. The linearized form of the Langmuir isotherm is as follows

$$q_e = \frac{q_{max} K_L C_e}{1 + K_L C_e} \quad (7)$$

where q_{max} is the maximum amount of drug adsorbed by a complete monolayer, q_e is the equilibrium drug uptake (in mg/g), C_e is the equilibrium concentration of the drug (in mg/L), and K_L is the equilibrium constant of adsorption (L/kg). The plot of C_e/q_e versus C_e forms a linear curve, for which the constants, q_{max} and K_L, are calculated.[71] Furthermore, the Langmuir adsorption isotherm for the ciprofloxacin drug at various temperatures is shown in Figure 7. The maximum drug uptake was found to decrease from 270.3 to 227.3 mg/g as the temperature increased from 290 to 303 K. Likewise, the equilibrium constant (K_L) values decreased as the temperature increased (Table 3). Obviously, as the temperature increased, the kinetic energy of the drug molecules increased and also the kinetic energy of the surface of the adsorbent increased, which weakened the drug adsorption and led to fewer drug molecules adsorbed on the hot surfaces of the adsorbent.

On the other hand, the Freundlich isotherm equation is as follows

$$q_e = K_F C_e^{\,n} \quad (8)$$

where q_e is the equilibrium uptake (mg/g), K_F is the Freundlich constant related to the adsorption capacity ($(mg^{(1-1/n)} L^{(1/n)})/g$), C_e is the equilibrium concentration of the drug (mg/L), and n is the heterogeneity factor.[77] The plot of ln q_e versus ln C_e forms a linear curve.[71] Table 3 shows the Freundlich parameters along with the correlation coefficients (R^2).

For the Temkin isotherm, the linear form is as follows

$$q_e = B_T \ln K_T + B_T \ln C_e \quad (9)$$

where q_e is the equilibrium uptake (mg/g), $B_T = RT/b_T$, where b_T is the Temkin constant related to the heat of adsorption (J/mol), R is the universal gas constant (8.314 J/mol.K), T is the temperature (K), C_e is the equilibrium concentration of the drug (in mg/L), and K_T is the maximum binding energy constant (L/mg). The plot of q_e versus ln C_e forms a linear curve.[71] Table 3 illustrates the adsorption isotherm parameters along with the correlation coefficients (R^2). As can be noted, all three models could fit the experimental data.

The Dubinin–Radushkevich (D–R) linear form is as follows

$$\ln q_e = \ln q_{max} - \beta\varepsilon^2 \quad (10)$$

where q_e is the equilibrium uptake (mg/g), β is the mean free energy (mol^2/kJ^2), ε is the Polanyi potential $= RT \ln\left(1 + \frac{1}{C_e}\right)$, where R is the universal gas constant (8.314 J/mol.K), T is the temperature (K), C_e is the equilibrium concentration of the drug (in mg/L), and E is the free energy (kJ/mol) equal to $1/\sqrt{2\beta}$. The plot of q_e versus ε^2 forms a linear curve.[78] Experimental determination of ciprofloxacin uptake by various adsorbents is discussed in Table 4.

Table 4. Ciprofloxacin Uptakes Using Different Adsorbents

adsorbent	maximum uptake (mg/g)	reference literature
sodium alginate/graphene oxide	86.12	79
activated carbon	300	80
carbon nanotubes	140	
carbon xerogel	280	
Fe-pillared clays	122.1	81
graphene oxide	379	82
carbon nanotubes	190	83
carbon nanotubes	120	84
TiO_2 nanotube/graphene oxide	181.8	85
magnetic chitosan-grafted GO	282.9	86
graphene	156.7	87
granular activated carbon	68	
cupric oxide nanoparticles	73.86	88

Ciprofloxacin Eradication Thermodynamics. Many important outputs can be extracted from the thermodynamic parameters, such as how strongly the adsorbate attaches to the surface of the adsorbent (i.e., chemisorption or physisorption process), exothermic or endothermic processes, and entropic changes that occur throughout the adsorption process. The adsorption process is considered to be physisorption when the ΔG° value is around 20 kJ/mol and chemisorption when the value is 80–400 kJ/mol.[89] Results of ciprofloxacin removal illustrated in Table 5 suggest that the adsorption of the drug on the nanohybrid adsorbent is physisorption. The thermodynamic parameters could be determined using eq 10 as follows

$$\ln K_L = -\frac{\Delta H^\circ}{RT} + \frac{\Delta S^\circ}{R} \quad (11)$$

Table 5. Thermodynamic Parameters for Ciprofloxacin Removal

temperature (K)	q_{max}[a] (mg/g)	equilibrium constant (K_L)[a]	ΔG° (kJ/mol)	ΔH° (kJ/mol)	ΔS° (J/mol K)
290	270.0	3.16×10^5	−30.53	−27.07	11.82
298	250.0	2.22×10^5	−30.50		
303	227.3	1.97×10^5	−30.71		

[a] q_{max} and K_L values were determined from the Langmuir adsorption isotherm.

https://dx.doi.org/10.1021/acsomega.9b03636
ACS Omega 2020, 5, 4457–4468

where K_L is the equilibrium constant determined from the Langmuir adsorption isotherms, R is the universal gas constant, T is the absolute temperature of adsorption (K). The plot of $\ln K_L$ versus reciprocal temperature ($1/T$) yields the enthalpy change (ΔH°) and entropy change (ΔS°) from the slope and intercept, respectively (Figure 7F), and the Gibbs free energy (ΔG°) values are calculated from $\Delta G^\circ = -RT \ln K_L$.[90]

Furthermore, the exothermic enthalpy change (ΔH°) value pointed to the successful bond formation of the drug with the nanohybrid adsorbent at the interface, and the positive entropy change (ΔS°) value indicated an entropy increase as a result of the adsorption process.[91]

CONCLUSIONS

In this article, new nanohybrid adsorbents were synthesized and characterized for ultimate eradication of the ciprofloxacin antibiotic from aqueous solutions. Nanohybrid GO/O-CNTs was composed of graphene oxide (GO) cross-linked via calcium ions (Ca^{2+}) with oxidized carbon nanotubes (O-CNTs) in a water-dispersed Tween 80 solution. The nanohybrid adsorbents were characterized using spectroscopic, thermal, and microscopic (FTIR, TGA, DTG, XRD, and SEM) techniques. The new nanohybrid was validated for ultimate eradication of the ciprofloxacin antibiotic from aqueous solutions. The ciprofloxacin antibiotic drug is medically prescribed in millions of medical prescriptions every year and hence exists in sewage treatment effluents, wastewaters, and domestic waters. Optimum parameters were validated for the eradication process, such as contact time, nanohybrid mass, solution temperature, solution pH, %cross-linking agent, and GO/O-CNT ratio. Ciprofloxacin removal dynamics displayed a pseudo-second-order fit with an intraparticle diffusion mechanism. Thermodynamic parameters of ciprofloxacin removal revealed a physisorption process and confirmed a simple desorption process. Our results provided outstanding drug eradication of up to 99.2% and ultimate drug uptake of 512 mg/g. In conclusion, the ultimate eradication of drugs from aqueous solutions is a proactive step in the right direction against the generated antimicrobial resistance (AMR) in the human body that may increase with time and, eventually, lead to disastrous deaths and epidemics.

AUTHOR INFORMATION

Corresponding Authors

Mohammad M. Fares − *Department of Chemistry, Faculty of Science & Arts, Jordan University of Science and Technology, Irbid 22110, Jordan;* orcid.org/0000-0002-0614-182X; Email: fares@just.edu.jo

Fahmi A. Abu Al-Rub − *Department of Chemical Engineering, Faculty of Engineering, Jordan University of Science and Technology, Irbid 22110, Jordan*; Email: abualrub@just.edu.jo

Author

Ahmad R. Mohammad − *Department of Chemical Engineering, Faculty of Engineering, Jordan University of Science and Technology, Irbid 22110, Jordan*

Complete contact information is available at: https://pubs.acs.org/10.1021/acsomega.9b03636

Notes

The authors declare no competing financial interest.

ACKNOWLEDGMENTS

The authors wish to acknowledge Jordan University of Science & Technology, project number: 49/2019, for financial support and facilities.

REFERENCES

(1) Crane, M.; Watts, C.; Boucard, T. Chronic aquatic environmental risks from exposure to human pharmaceuticals. *Sci. Total Environ.* **2006**, *367*, 23−41.

(2) Ezechiáš, M.; Janochová, J.; Filipová, A.; Křesinová, Z.; Cajthaml, T. Widely used pharmaceuticals present in the environment revealed as in vitro antagonists for human estrogen and androgen receptors. *Chemosphere* **2016**, *152*, 284−291.

(3) Novo, A.; André, S.; Viana, P.; Nunes, O. C.; Manaia, C. M. Antibiotic resistance, antimicrobial residues and bacterial community composition in urban wastewater. *Water Res.* **2013**, *47*, 1875−1887.

(4) Yang, W.; Zhou, H.; Cicek, N. Treatment of organic micropollutants in water and wastewater by UV-based processes: a literature review. *Crit. Rev. Environ. Sci. Technol.* **2014**, *44*, 1443−1476.

(5) Gavrilescu, M.; Demnerová, K.; Aamand, J.; Agathos, S.; Fava, F. Emerging pollutants in the environment: present and future challenges in biomonitoring, ecological risks and bioremediation. *New Biotechnol.* **2015**, *32*, 147−156.

(6) Qiao, M.; Ying, G. G.; Singer, A. C.; Zhu, Y. G. Review of antibiotic resistance in China and its environment. *Environ. Int.* **2018**, *110*, 160−172.

(7) Khodadadi, M.; Ehrampoush, M.; Ghaneian, M.; Allahresani, A.; Mahvi, A. Synthesis and characterizations of FeNi 3 @SiO 2 @TiO 2 nanocomposite and its application in photo- catalytic degradation of tetracycline in simulated wastewater. *J. Mol. Liq.* **2018**, *255*, 224−232.

(8) Desbiolles, F.; Malleret, L.; Tiliacos, C.; Wong-Wah-Chung, P.; Laffont-Schwob, I. Occurrence and ecotoxicological assessment of pharmaceuticals: Is there a risk for the Mediterranean aquatic environment? *Sci. Total Environ.* **2018**, *639*, 1334−1348.

(9) Wishart, D. S.; Feunang, Y. D.; Guo, A. C.; Lo, E. J.; Marcu, A.; Grant, J. R.; Sajed, T.; Johnson, D.; Li, C.; Sayeeda, Z.; Assempour, N.; et al. DrugBank 5.0: a major update to the DrugBank database for 2018. *Nucleic Acids Res.* **2018**, *46*, D1074−D1082.

(10) Kumar, A.; Pal, D. Antibiotic resistance and wastewater: correlation, impact and critical human health challenges. *J. Environ. Chem. Eng.* **2018**, *6*, 52−58.

(11) Stalder, T.; Barraud, O.; Casellas, M.; Dagot, C.; Ploy, M. C. Integron involvement in environmental spread of antibiotic resistance. *Front. Microbiol.* **2012**, *3*, 119.

(12) Gaw, S.; Thomas, K. V.; Hutchinson, T. H. Sources, impacts and trends of pharmaceuticals in the marine and coastal environment. *Philos. Trans. R. Soc. B* **2014**, *369*, No. 20130572.

(13) Kumar, M.; Jaiswal, S.; Sodhi, K. K.; Shree, P.; Singh, D. K.; Agrawal, P. K.; Shukla, P. Antibiotics bioremediation: Perspectives on its ecotoxicity and resistance. *Environ. Int.* **2019**, *124*, 448−461.

(14) Jasovský, D.; Littmann, J.; Zorzet, A.; Cars, O. Antimicrobial resistance—a threat to the world's sustainable development. *Upsala J. Med. Sci.* **2016**, *121*, 159−164.

(15) Sugden, R.; Kelly, R.; Davies, S. Combatting antimicrobial resistance globally. *Nat. Microbiol.* **2016**, *1*, No. 16187.

(16) Tiwari, B.; Sellamuthu, B.; Ouarda, Y.; Drogui, P.; Tyagi, R. D.; Buelna, G. Review on fate and mechanism of removal of pharmaceutical pollutants from wastewater using biological approach. *Bioresour. Technol.* **2017**, *224*, 1−12.

(17) Niemuth, N. J.; Klaper, R. D. Emerging wastewater contaminant metformin causes intersex and reduced fecundity in fish. *Chemosphere* **2015**, *135*, 38−45.

(18) Oaks, J. L.; Gilbert, M.; Virani, M. Z.; Watson, R. T.; Meteyer, C. U.; Rideout, B. A.; Shivaprasad, H. L.; Ahmed, S.; Chaudhry, M. J. I.; Arshad, M.; Mahmood, S.; et al. Diclofenac residues as the cause of vulture population decline in Pakistan. *Nature* **2004**, *427*, 630.

(19) Redgrave, L. S.; Sutton, S. B.; Webber, M. A.; Piddock, L. J. Fluoroquinolone resistance: mechanisms, impact on bacteria, and role in evolutionary success. *Trends Microbiol.* **2014**, *22*, 438−445.
(20) ClinCalc DrugStats Database. The Top 300 of 2019. 2019, https://clincalc.com/DrugStats/Top300Drugs.aspx (accessed 3 June 2019).
(21) Kelly, K. R.; Brooks, B. W. Global aquatic hazard assessment of ciprofloxacin: exceedances of antibiotic resistance development and ecotoxicological thresholds. *Prog. Mol. Biol. Transl. Sci.* **2018**, *159*, 59−77.
(22) Riemenschneider, C.; Al-Raggad, M.; Moeder, M.; Seiwert, B.; Salameh, E.; Reemtsma, T. Pharmaceuticals, their metabolites, and other polar pollutants in field-grown vegetables irrigated with treated municipal wastewater. *J. Agric. Food Chem.* **2016**, *64*, 5784−5792.
(23) Papageorgiou, M.; Kosma, C.; Lambropoulou, D. Seasonal occurrence, removal, mass loading and environmental risk assessment of 55 pharmaceuticals and personal care products in a municipal wastewater treatment plant in Central Greece. *Sci. Total Environ.* **2016**, *543*, 547−569.
(24) Pereira, A. M.; Silva, L. J.; Meisel, L. M.; Lino, C. M.; Pena, A. Environmental impact of pharmaceuticals from Portuguese wastewaters: geographical and seasonal occurrence, removal and risk assessment. *Environ. Res.* **2015**, *136*, 108−119.
(25) Kostich, M. S.; Batt, A. L.; Lazorchak, J. M. Concentrations of prioritized pharmaceuticals in effluents from 50 large wastewater treatment plants in the US and implications for risk estimation. *Environ. Pollut.* **2014**, *184*, 354−359.
(26) Zhang, Y.; Cai, X.; Lang, X.; Qiao, X.; Li, X.; Chen, J. Insights into aquatic toxicities of the antibiotics oxytetracycline and ciprofloxacin in the presence of metal: complexation versus mixture. *Environ. Pollut.* **2012**, *166*, 48−56.
(27) Blair, B.; Nikolaus, A.; Hedman, C.; Klaper, R.; Grundl, T. Evaluating the degradation, sorption, and negative mass balances of pharmaceuticals and personal care products during wastewater treatment. *Chemosphere* **2015**, *134*, 395−401.
(28) Narumiya, M.; Nakada, N.; Yamashita, N.; Tanaka, H. Phase distribution and removal of pharmaceuticals and personal care products during anaerobic sludge digestion. *J. Hazard. Mater.* **2013**, *260*, 305−312.
(29) Nguyen, L. N.; Hai, F. I.; Yang, S.; Kang, J.; Leusch, F. D.; Roddick, F.; Nghiem, L. D.; Price, W. E. Removal of pharmaceuticals, steroid hormones, phytoestrogens, UV-filters, industrial chemicals and pesticides by Trametes versicolor: role of biosorption and biodegradation. *Int. Biodeterior. Biodegrad.* **2014**, *88*, 169−175.
(30) Noutsopoulos, C.; Mamais, D.; Mpouras, T.; Kokkinidou, D.; Samaras, V.; Antoniou, K.; Gioldasi, M. The role of activated carbon and disinfection on the removal of endocrine disrupting chemicals and non-steroidal anti-inflammatory drugs from wastewater. *Environ. Technol.* **2014**, *35*, 698−708.
(31) Michael, I.; Rizzo, L.; McArdell, C. S.; Manaia, C. M.; Merlin, C.; Schwartz, T.; Fatta-Kassinos, D. Urban wastewater treatment plants as hotspots for the release of antibiotics in the environment: a review. *Water Res.* **2013**, *47*, 957−995.
(32) Ali, I.; Asim, M.; Khan, T. A. Low cost adsorbents for the removal of organic pollutants from wastewater. *J. Environ. Manage.* **2012**, *113*, 170−183.
(33) Das, R.; Hamid, S. B. A.; Ali, M. E.; Ismail, A. F.; Annuar, M. S. M.; Ramakrishna, S. Multifunctional carbon nanotubes in water treatment: the present, past and future. *Desalination* **2014**, *354*, 160−179.
(34) Iijima, S. Carbon nanotubes: past, present, and future. *Phys. B* **2002**, *323*, 1−5.
(35) Qu, X.; Alvarez, P. J.; Li, Q. Applications of nanotechnology in water and wastewater treatment. *Water Res.* **2013**, *47*, 3931−3946.
(36) Dalton, A. B.; Collins, S.; Razal, J.; Munoz, E.; Ebron, V. H.; Kim, B. G.; Coleman, J. N.; Ferraris, J. P.; Baughman, R. H. Continuous carbon nanotube composite fibers: properties, potential applications, and problems. *J. Mater. Chem.* **2004**, *14*, 1−3.
(37) Jung, C.; Son, A.; Her, N.; Zoh, K. D.; Cho, J.; Yoon, Y. Removal of endocrine disrupting compounds, pharmaceuticals, and personal care products in water using carbon nanotubes: A review. *J. Ind. Eng. Chem.* **2015**, *27*, 1−11.
(38) Shan, D.; Deng, S.; Zhao, T.; Yu, G.; Winglee, J.; Wiesner, M. R. Preparation of regenerable granular carbon nanotubes by a simple heating-filtration method for efficient removal of typical pharmaceuticals. *Chem. Eng. J.* **2016**, *294*, 353−361.
(39) Chang, H.; Wu, H. Graphene-based nanocomposites: preparation, functionalization, and energy and environmental applications. *Energy Environ. Sci.* **2013**, *6*, 3483−3507.
(40) Tang, Y.; Guo, H.; Xiao, L.; Yu, S.; Gao, N.; Wang, Y. Synthesis of reduced graphene oxide/magnetite composites and investigation of their adsorption performance of fluoroquinolone antibiotics. *Colloids Surf., A* **2013**, *424*, 74−80.
(41) Kyzas, G. Z.; Koltsakidou, A.; Nanaki, S. G.; Bikiaris, D. N.; Lambropoulou, D. A. Removal of beta-blockers from aqueous media by adsorption onto graphene oxide. *Sci. Total Environ.* **2015**, *537*, 411−420.
(42) Mura, S.; Jiang, Y.; Vassalini, I.; Gianoncelli, A.; Alessandri, I.; Granozzi, G.; Calvillo, L.; Senes, N.; Enzo, S.; Innocenzi, P.; Malfatti, L. Graphene Oxide/Iron Oxide Nanocomposites for Water Remediation. *ACS Appl. Nano Mater.* **2018**, *1*, 6724−6732.
(43) Thakur, K.; Kandasubramanian, B. Graphene and Graphene Oxide-Based Composites for Removal of Organic Pollutants. *J. Chem. Eng. Data* **2019**, *64*, 833−867.
(44) Yao, N.; Zhang, X.; Yang, Z.; Yang, W.; Tian, Z.; Zhang, L. Norfloxacin and Bisphenol-A Removal Using Temperature-Switchable Graphene Oxide. *ACS Appl. Mater. Interfaces* **2018**, *10*, 29083−29091.
(45) Delhiraja, K.; Vellingiri, K.; Boukhvalov, D. W.; Philip, L. Development of highly water stable graphene oxide based composites for the removal of pharmaceuticals and personal care products. *Ind. Eng. Chem. Res.* **2019**, 2899−2913.
(46) Barroso-Bujans, F.; Cerveny, S.; Verdejo, R.; del Val, J. D.; Alberdi, J. M.; Alegría, A.; Colmenero, J. Permanent adsorption of organic solvents in graphite oxide and its effect on the thermal exfoliation. *Carbon* **2010**, *48*, 1079−1087.
(47) Hummers, W. S.; Offeman, R. E. Preparation of graphite oxide. *J. Am. Chem. Soc.* **1958**, *80*, 1339.
(48) Zaaba, N. I.; Foo, K. L.; Hashim, U.; Tan, S. J.; Liu, W. W.; Voon, C. H. Synthesis of graphene oxide using modified hummers method: solvent influence. *Proc. Eng.* **2017**, *184*, 469−477.
(49) Fares, M. M.; Al-Rub, F. A. A.; Massadeh, K. A. H. Lightweight MWCNTs-g-PAN Carbon Fiber Precursors. Sensitive High Absorptivity and Novel Wide-Bandgap Conjugated Polymers. *Ind. Eng. Chem. Res.* **2015**, *54*, 9064−9071.
(50) Fares, M. M. π-Plasmon absorbance films of carboxylic functionalized CNT s coupled with renewable PGP platforms. *Polym. Adv. Technol.* **2018**, *29*, 1861−1869.
(51) Kuo, C. Y. Desorption and re-adsorption of carbon nanotubes: Comparisons of sodium hydroxide and microwave irradiation processes. *J. Hazard. Mater.* **2008**, *152*, 949−954.
(52) Lerf, A.; He, H.; Forster, M.; Klinowski, J. Structure of graphite oxide revisited. *J. Phys. Chem. B* **1998**, *102*, 4477−4482.
(53) Wang, G.; Yang, Z.; Li, X.; Li, C. Synthesis of poly (aniline-co-o-anisidine)-intercalated graphite oxide composite by delamination/reassembling method. *Carbon* **2005**, *43*, 2564−2570.
(54) Stankovich, S.; Dikin, D. A.; Piner, R. D.; Kohlhaas, K. A.; Kleinhammes, A.; Jia, Y.; Wu, Y.; Nguyen, S. T.; Ruoff, R. S. Synthesis of graphene-based nanosheets via chemical reduction of exfoliated graphite oxide. *carbon* **2007**, *45*, 1558−1565.
(55) Yang, H.; Shan, C.; Li, F.; Han, D.; Zhang, Q.; Niu, L. Covalent functionalization of polydispersechemically-converted graphene sheets with amine-terminated ionic liquid. *Chem. Commun.* **2009**, *26*, 3880−3882.
(56) Datsyuk, V.; Kalyva, M.; Papagelis, K.; Parthenios, J.; Tasis, D.; Siokou, A.; Kallitsis, I.; Galiotis, C. Chemical oxidation of multiwalledarbonnanotubes. *Carbon* **2008**, *46*, 833−840.

https://dx.doi.org/10.1021/acsomega.9b03636
ACS Omega 2020, 5, 4457−4468

(57) González, M.; Baselga, J.; Pozuelo, J. Modulating the electromagnetic shielding mechanisms by thermal treatment of high porosity graphene aerogels. *Carbon* **2019**, *147*, 27−34.
(58) Luo, C.; Jiao, T.; Gu, J.; Tang, Y.; Kong, J. Graphene shield by SiBCN ceramic: a promising high-temperature electromagnetic wave-absorbing material with oxidation resistance. *ACS Appl. Mater. Interfaces* **2018**, *10*, 39307−39318.
(59) Ortiz, S. N. C.; Cabanzo, R.; Mejia-Ospino, E. Crude oil/water emulsion separation using graphene oxide and amine-modified graphene oxide particles. *Fuel* **2019**, *240*, 162−168.
(60) Saleh, T. A. The influence of treatment temperature on the acidity of MWCNT oxidized by HNO3 or a mixture of HNO3/H2SO4. *Appl. Surf. Sci.* **2011**, *257*, 7746−7751.
(61) Kong, L.; Yin, X.; Xu, H.; Yuan, X.; Wang, T.; Xu, Z.; Huang, J.; Yang, R.; Fan, H. Powerful absorbing and lightweight electromagnetic shielding CNTs/RGO composite. *Carbon* **2019**, *145*, 61−66.
(62) Geng, Y.; Wang, S. J.; Kim, J. K. Preparation of graphite nanoplatelets and graphene sheets. *J. Colloid Interface Sci.* **2009**, *336*, 592−598.
(63) Jiang, L.; Liu, Y.; Liu, S.; Hu, X.; Zeng, G.; Hu, X.; Liu, S.; Liu, S.; Huang, B.; Li, M. Fabrication of β-cyclodextrin/poly (l-glutamic acid) supported magnetic graphene oxide and its adsorption behavior for 17β-estradiol. *Chem. Eng. J.* **2017**, *308*, 597−605.
(64) Ramesha, G. K.; Kumara, A. V.; Muralidhara, H. B.; Sampath, S. Graphene and graphene oxide as effective adsorbents toward anionic and cationic dyes. *J. Colloid Interface Sci.* **2011**, *361*, 270−277.
(65) Alexandratos, V. G.; Elzinga, E. J.; Reeder, R. J. Arsenate uptake by calcite: macroscopic and spectroscopic characterization of adsorption and incorporation mechanisms. *Geochim. Cosmochim. Acta* **2007**, *71*, 4172−4187.
(66) Bhatti, H. N.; Nasir, A. W.; Hanif, M. A. Efficacy of Daucuscarota L. waste biomass for the removal of chromium from aqueous solutions. *Desalination* **2010**, *253*, 78−87.
(67) Jalil, M. E. R.; Baschini, M.; Sapag, K. Influence of pH and antibiotic solubility on the removal of ciprofloxacin from aqueous media using montmorillonite. *Appl. Clay Sci.*. **2015**, *114*, 69−76.
(68) Serrano-Aroca, Á.; Ruiz-Pividal, J. F.; Llorens-Gámez, M. Enhancement of water diffusion and compression performance of crosslinked alginate films with a minuscule amount of graphene oxide. *Sci. Rep.* **2017**, *7*, No. 11684.
(69) Núñez, D. J.; Benito, A. M.; Rouzière, S.; Launois, P.; Arenal, R.; Ajayan, P. M.; Maser, W. K. Graphene oxide−carbon nanotube hybrid assemblies: Cooperatively strengthened OH··· O5C hydrogen bonds and removal of chemisorbed water. *Chem. Sci.* **2017**, *8*, 4987−4995.
(70) Xu, J.; Wang, L.; Zhu, Y. Decontamination of bisphenol A from aqueous solution by graphene adsorption. *Langmuir* **2012**, *28*, 8418−8425.
(71) Hu, X. J.; Wang, J. S.; Liu, Y. G.; Li, X.; Zeng, G. M.; Bao, Z. L.; Zeng, X. X.; Chen, A. W.; Long, F. Adsorption of chromium (VI) by ethylenediamine-modified cross-linked magnetic chitosan resin: isotherms, kinetics and thermodynamics. *J. Hazard. Mater.* **2011**, *185*, 306−314.
(72) Tanzifi, M.; Yaraki, M. T.; Kiadehi, A. D.; Hosseini, S. H.; Olazar, M.; Bharti, A. K.; Agarwal, S.; Gupta, V. K.; Kazemi, A. Adsorption of Amido Black 10B from aqueous solution using polyaniline/SiO2 nanocomposite: Experimental investigation and artificial neural network modeling. *J. Colloid Interface Sci.* **2018**, *510*, 246−261.
(73) Weber, W. J.; Morris, J. C. Kinetics of adsorption on carbon from solution. *J. Sanit. Eng. Div.* **1963**, *89*, 31−60.
(74) Boyd, G. E.; Adamson, A. W.; Myers, L. S., Jr The exchange adsorption of ions from aqueous solutions by organic zeolites. II. Kinetics1. *J. Am. Chem. Soc.* **1947**, *69*, 2836−2848.
(75) Djeribi, R.; Hamdaoui, O. Sorption of copper (II) from aqueous solutions by cedar sawdust and crushed brick. *Desalination* **2008**, *225*, 95−112.
(76) Wu, Z.; Zhong, H.; Yuan, X.; Wang, H.; Wang, L.; Chen, X.; Zeng, G.; Wu, Y. Adsorptive removal of methylene blue by rhamnolipid-functionalized graphene oxide from wastewater. *Water Res.* **2014**, *67*, 330−344.
(77) Abu Al-Rub, F. A. Biosorption of zinc on palm tree leaves: equilibrium, kinetics, and thermodynamics studies. *Sep. Sci. Technol.* **2006**, *41*, 3499−3515.
(78) Chaudhry, S.; Zaidi, Z.; Siddiqui, S. Isotherm, kinetic and thermodynamics of arsenic adsorption onto Iron-Zirconium Binary Oxide-Coated Sand (IZBOCS): Modelling and process optimization. *J. Mol. Liq.* **2017**, *229*, 230−240.
(79) Fei, Y.; Li, Y.; Han, S.; Ma, J. Adsorptive removal of ciprofloxacin by sodium alginate/graphene oxide composite beads from aqueous solution. *J. Colloid Interface Sci.* **2016**, *484*, 196−204.
(80) Carabineiro, S. A. C.; Thavorn-Amornsri, T.; Pereira, M. F. R.; Figueiredo, J. L. Adsorption of ciprofloxacin on surface-modified carbon materials. *Water Res.* **2011**, *45*, 4583−4591.
(81) Roca Jalil, M.; Baschini, M.; Sapag, K. Removal of ciprofloxacin from aqueous solutions using pillared clays. *Materials* **2017**, *10*, 1345.
(82) Chen, H.; Gao, B.; Li, H. Removal of sulfamethoxazole and ciprofloxacin from aqueous solutions by graphene oxide. *J. Hazard. Mater.* **2015**, *282*, 201−207.
(83) Yu, F.; Sun, S.; Han, S.; Zheng, J.; Ma, J. Adsorption removal of ciprofloxacin by multi-walled carbon nanotubes with different oxygen contents from aqueous solutions. *Chem. Eng. J.* **2016**, *285*, 588−595.
(84) Li, H.; Zhang, D.; Han, X.; Xing, B. Adsorption of antibiotic ciprofloxacin on carbon nanotubes: pH dependence and thermodynamics. *Chemosphere* **2014**, *95*, 150−155.
(85) Zhuang, Y.; Yu, F.; Ma, J. Enhanced adsorption and removal of ciprofloxacin on regenerable long TiO 2 nanotube/graphene oxide hydrogel adsorbents. *J. Nanomater.* **2015**, *2015*, 4.
(86) Wang, F.; Yang, B.; Wang, H.; Song, Q.; Tan, F.; Cao, Y. Removal of ciprofloxacin from aqueous solution by a magnetic chitosan grafted graphene oxide composite. *J. Mol. Liq.* **2016**, *222*, 188−194.
(87) Zhu, X.; Tsang, D. C.; Chen, F.; Li, S.; Yang, X. Ciprofloxacin adsorption on graphene and granular activated carbon: kinetics, isotherms, and effects of solution chemistry. *Environ. Technol.* **2015**, *36*, 3094−3102.
(88) Ahmadi, S.; Banach, A.; Mostafapour, F. K. Study survey of cupric oxide nanoparticles in removal efficiency of ciprofloxacin antibiotic from aqueous solution: Adsorption isotherm study. *Desal. Water Treat.* **2017**, *89*, 297−303.
(89) Wu, Y.; Luo, H.; Wang, H.; Wang, C.; Zhang, J.; Zhang, Z. Adsorption of hexavalent chromium from aqueous solutions by graphene modified with cetyltrimethylammonium bromide. *J. Colloid Interface Sci.* **2013**, *394*, 183−191.
(90) Mahmoud, M. E.; Nabil, G. M.; El-Mallah, N. M.; Bassiouny, H. I.; Kumar, S.; Abdel-Fattah, T. M. Kinetics, isotherm, and thermodynamic studies of the adsorption of reactive red 195 A dye from water by modified Switchgrass Biochar adsorbent. *J. Ind. Eng. Chem.* **2016**, *37*, 156−167.
(91) Almeida, C. A. P.; Debacher, N. A.; Downs, A. J.; Cottet, L.; Mello, C. A. D. Removal of methylene blue from colored effluents by adsorption on montmorillonite clay. *J. Colloid Interface Sci.* **2009**, *332*, 46−53.

https://dx.doi.org/10.1021/acsomega.9b03636
ACS Omega 2020, 5, 4457−4468